Rapid Communications

# Spontaneous deformation of flexible ferromagnetic ribbons induced by Dzyaloshinskii-Moriya interaction

Kostiantyn V. Yershov,[1,2,*] Volodymyr P. Kravchuk,[1,2,3,†] Denis D. Sheka,[4,‡] Jeroen van den Brink,[2,5,6,§] and Yuri Gaididei[1,‖]

[1]*Bogolyubov Institute for Theoretical Physics of National Academy of Sciences of Ukraine, 03143 Kyiv, Ukraine*
[2]*Leibniz-Institut für Festkörper- und Werkstoffforschung, IFW Dresden, D-01171 Dresden, Germany*
[3]*Institut für Theoretische Festkörperphysik, Karlsruher Institut für Technologie, D-76131 Karlsruhe, Germany*
[4]*Taras Shevchenko National University of Kyiv, 01601 Kyiv, Ukraine*
[5]*Institute for Theoretical Physics, TU Dresden, 01069 Dresden, Germany*
[6]*Department of Physics, Washington University, St. Louis, Missouri 63130, USA*

(Received 17 July 2019; revised manuscript received 13 September 2019; published 11 October 2019)

Here, we predict the effect of the spontaneous deformation of a flexible ferromagnetic ribbon induced by Dzyaloshinskii-Moriya interaction (DMI). The geometrical form of the deformation is determined both by the type of DMI and by the equilibrium magnetization of the stripe. We found three different geometrical phases, namely, (i) the DNA-like deformation with the stripe central line in the form of a helix, (ii) the helicoid deformation with the straight central line, and (iii) cylindrical deformation. In the main approximation the magnitude of the DMI-induced deformation is determined by the ratio of the DMI constant and the Young's modulus. It can be effectively controlled by the external magnetic field, which can be utilized for the nanorobotics applications. All analytical calculations are confirmed by numerical simulations.

DOI: 10.1103/PhysRevB.100.140407

*Introduction.* Magnetic soft matter opens new possibilities in the construction and fabrication of shapeable magnetoelectronics [1,2], interactive human-machine interfaces [3,4], and programmable magnetic materials [5,6]. Remote control of the shape and three-dimensional (3D) navigation of the soft magnet by means of the external magnetic field stimulate intensive investigations in the area of milli- [4–8] and microrobotics [9–11] for flexible electronics and biomedical applications. So far the magnetosensitive elastomers [12–17] are the most studied magnetically responsive flexible materials. The magnetic properties of elastomers are determined by the long-range dipole-dipole interaction [18–21] which results in the relatively large scale of the geometrical deformations. It is well known that organic, organic-inorganic hybrid, and molecule-based magnets exhibit different types of magnetic ordering [22–29] and some of them can keep ferromagnetic order even for a room temperature [30]. In comparison with elastomers, the dominant interaction in the molecule-based magnets is a local short-range exchange interaction. Therefore, the scale of deformations in such systems is in nanoscale range which allows one to significantly reduce the size of the object. The submicrometer size of the molecule-based magnets and the possibility to control the geometry of the magnet by means of magnetic field opens new possibilities in the development of *nanorobots* in the context of organic electronics and spintronics [31].

Deformation of a flexible magnet induced by its magnetization subsystem was predicted in a number of previous works [32–35]. Here, we demonstrate that a presence of intrinsic Dzyaloshinskii-Moriya interaction (DMI) results in a spontaneous deformation of a flexible magnetic ribbon. Depending on the mechanical, magnetic, and geometric parameters, and the symmetry of the DMI one can obtain different equilibrium states (see Table I). A promising feature of the DMI-induced deformation is its field-controlled reconfigurability, which is an important issue for the nanorobotics applications. The numerical simulations confirm our analytical calculations: shape of the deformed ribbon and phase diagram of equilibrium states. We used an in-house developed simulating code, which takes into account both magnetic and geometrical degrees of freedom.

*Model.* We consider a 3D narrow ferromagnetic ribbon of rectangular cross section whose thickness $h$ and width $w$ are small enough to ensure the magnetization uniformity along a ribbon cross section. The ribbon length $L$ is substantially larger than the transversal dimensions ($h \ll w \ll L$). The space domain occupied by the ribbon is defined as $\boldsymbol{r}(\xi_1, \xi_2, \eta) = \boldsymbol{\varsigma}(\xi_1, \xi_2) + \eta\, \boldsymbol{n}(\xi_1, \xi_2)$. Here, $\boldsymbol{\varsigma}$ determines a 2D surface $\mathcal{S}$ embedded in $\mathbb{R}^3$ with $\xi_1 \in [0, L]$ and $\xi_2 \in [-w/2, w/2]$ being local curvilinear coordinates on $\mathcal{S}$. The unit vector $\boldsymbol{n}$ denotes the surface normal and the parameter $\eta \in [-h/2, h/2]$ is the curvilinear coordinate along the normal direction. The parametrization $\boldsymbol{\varsigma}(\xi_1, \xi_2)$ induces the natural tangential basis $\boldsymbol{g}_\alpha = \partial_\alpha \boldsymbol{\varsigma}$ with the corresponding metric tensor elements $g_{\alpha\beta} = \boldsymbol{g}_\alpha \cdot \boldsymbol{g}_\beta$. Here, $\alpha, \beta = 1, 2$ and $\partial_\alpha \equiv \partial_{\xi_\alpha}$. Assuming that vectors $\boldsymbol{g}_\alpha$ are orthogonal, one can introduce

*yershov@bitp.kiev.ua
†vkravchuk@bitp.kiev.ua
‡sheka@knu.ua
§j.van.den.brink@ifw-dresden.de
‖ybg@bitp.kiev.ua

 

TABLE I. Schematic illustrations of possible DMI-induced deformations of flexible ferromagnetic ribbon for different types of DMI and directions of the magnetization.

| Magnetization direction | DMI type: $\mathcal{E}_{\rm D}^{\rm B} = \boldsymbol{m}\cdot[\boldsymbol{\nabla}\times\boldsymbol{m}]$ | DMI type: $\mathcal{E}_{\rm D}^{\rm N} = m_n\boldsymbol{\nabla}\cdot\boldsymbol{m} - \boldsymbol{m}\cdot\boldsymbol{\nabla}m_n$ |
|---|---|---|
| $\boldsymbol{m} = \pm\boldsymbol{e}_1$ | DNA-like and helicoid states 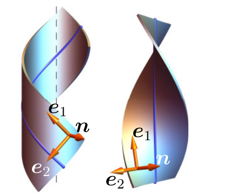 | Undeformed state 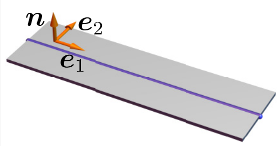 |
| $\boldsymbol{m} = \pm\boldsymbol{n}$ | Undeformed state 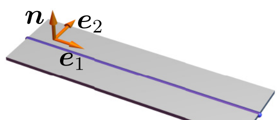 | Cylindrical state 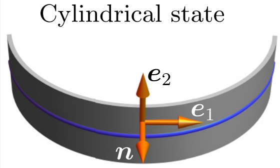 |



the orthonormal basis $\{\boldsymbol{e}_1, \boldsymbol{e}_2, \boldsymbol{n}\}$, where $\boldsymbol{e}_\alpha = \boldsymbol{g}_\alpha/\sqrt{g_{\alpha\alpha}}$ and $\boldsymbol{n} = \boldsymbol{e}_1 \times \boldsymbol{e}_2$ [see Figs. 1(a) and 1(b) for detailed notations].

The total energy $E = E_{\rm E} + E_{\rm M}$ of a flexible ferromagnetic ribbon is a summation of elastic [37,38],

$$E_{\rm E} = \frac{Y}{8(1+\nu)}\int_0^L\int_{-w/2}^{w/2}\left(h\mathcal{E}_{\rm S} + \frac{h^3}{3}\mathcal{E}_{\rm B}\right)\sqrt{g}\,d\xi_1 d\xi_2, \tag{1a}$$

and magnetic,

$$E_{\rm M} = h\int_0^L\int_{-w/2}^{w/2}(A\mathcal{E}_{\rm EX} + K\mathcal{E}_{\rm A} + D\mathcal{E}_{\rm D})\sqrt{g}\,d\xi_1 d\xi_2, \tag{1b}$$

energy terms. Elastic energy is taken for the case of thin amorphous films where only terms of first and third order of magnitude with respect to thickness $h$ are taken into account [37]. Here, $g = \det\|g_{\alpha\beta}\|$ and $\bar{g} = \det\|\bar{g}_{\alpha\beta}\|$ with $\bar{g}_{\alpha\beta}$ being the metric tensor for ribbon free of elastic tensions (we consider a straight ribbon with $\bar{g}_{\alpha\beta} = \delta_{\alpha\beta}$ as a reference metric). Parameters $Y$ and $\nu \in [0, 0.5]$ in (1a) are Young's modulus and Poisson ratio, respectively.

The first term in elastic energy (1a) determines stretching energy density $\mathcal{E}_{\rm S} = (\frac{\nu}{1-\nu}\bar{g}^{\alpha\beta}\bar{g}^{\gamma\delta} + \bar{g}^{\alpha\gamma}\bar{g}^{\beta\delta})(g_{\alpha\beta} - \bar{g}_{\alpha\beta})(g_{\gamma\delta} - \bar{g}_{\gamma\delta})$. The last term in (1a) corresponds to the bending energy $\mathcal{E}_{\rm B} = (\frac{\nu}{1-\nu}\bar{g}^{\alpha\beta}\bar{g}^{\gamma\delta} + \bar{g}^{\alpha\gamma}\bar{g}^{\beta\delta})b_{\alpha\beta}b_{\gamma\delta}$ with $b_{\alpha\beta} = \boldsymbol{n}\cdot\partial_\beta\boldsymbol{g}_\alpha$ being the second fundamental form.

The first term in (1b) is the exchange energy density with $\mathcal{E}_{\rm EX} = \sum_{i=x,y,z}(\partial_i\boldsymbol{m})^2$, and $A$ is an exchange constant. Here $\boldsymbol{m} = \boldsymbol{M}/M_s$ is the unit magnetization vector with $M_s$ being the saturation magnetization. The second term in (1b) is the anisotropy energy density $\mathcal{E}_{\rm A} = 1 - (\boldsymbol{m}\cdot\boldsymbol{e}_{\rm A})^2$ with $\boldsymbol{e}_{\rm A}$ being easy-axis vector. The vector $\boldsymbol{e}_{\rm A}$ follows either normal or tangential direction and in this way, the anisotropy term in (1b) realizes the magnetoelastic coupling. Parameter $K > 0$ is easy-axial anisotropy constant. The exchange-anisotropy competition results in the magnetic length $\ell = \sqrt{A/K}$, which determines the length scale of the system. The last term in (1b) represents DMI contribution $\mathcal{E}_{\rm D}$ with $D$ being the DMI constant. We consider two types of DMI: (i) $\mathcal{E}_{\rm D}^{\rm B} = \boldsymbol{m}\cdot[\boldsymbol{\nabla}\times\boldsymbol{m}]$ is typical for systems with $T$ symmetry [39]. In the following we call this DMI of Bloch type, since it results in the domain walls and skyrmions of Bloch type. (ii) $\mathcal{E}_{\rm D}^{\rm N} = m_n\boldsymbol{\nabla}\cdot\boldsymbol{m} - \boldsymbol{m}\cdot\boldsymbol{\nabla}m_n$ is typical for ultrathin films [40,41], bilayers [42], or materials belonging to the $C_{nv}$ crystallographic group. In the following we call this DMI of Néel type. Recently it was shown that Néel DMI can be obtained in the Janus monolayers of chromium trihalides $\mathrm{Cr(I,X)_3}$ [43]. It is also important to note that DMI was recently observed in amorphous GdFeCo films [44].

A DMI in a rigid magnetic system results in the appearance of periodical structures (e.g., conical or helical modulations [45–48]). In systems with strong enough anisotropy ($|D|/\sqrt{AK} < 4/\pi$) the periodical structures are suppressed and we have uniform magnetization distribution. However, if we add additional elastic degrees of freedom to the

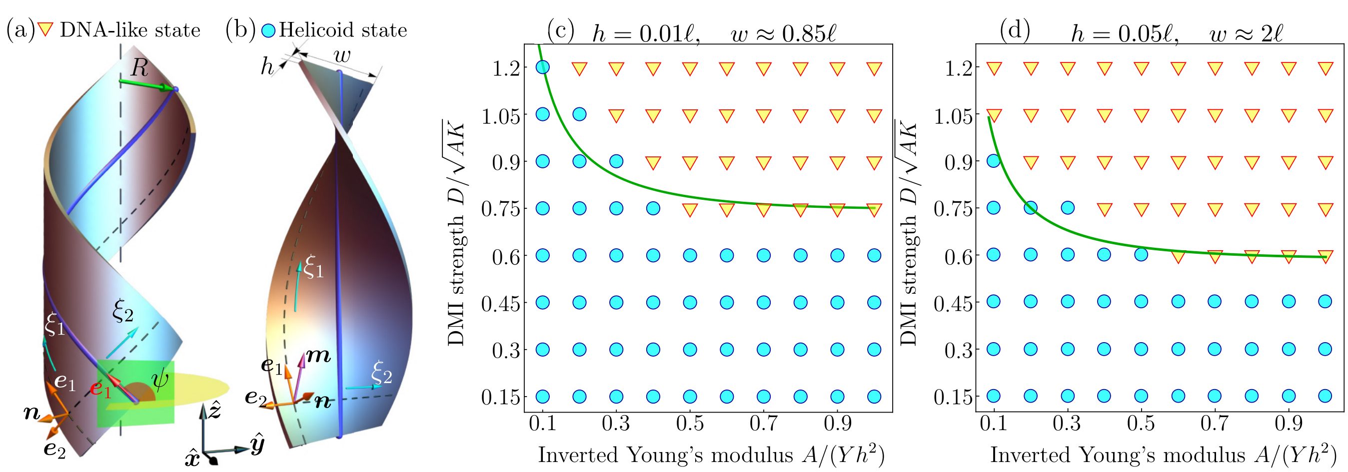


FIG. 1. Equilibrium states of flexible ferromagnetic ribbon with DMI in form $\mathcal{E}_{\rm D} = \mathcal{E}_{\rm D}^{\rm B}$: (a),(b) Shapes of DNA-like (a) and helicoid (b) states. (c) and (d) are phase diagrams of equilibrium states of the flexible ribbon. Symbols show the results of the numerical simulations: circles and triangles correspond to helicoid and DNA-like states, respectively. The thick green line in (c) and (d) describes the boundary between equilibrium states [36]. In all cases we have $\nu = 1/3$.

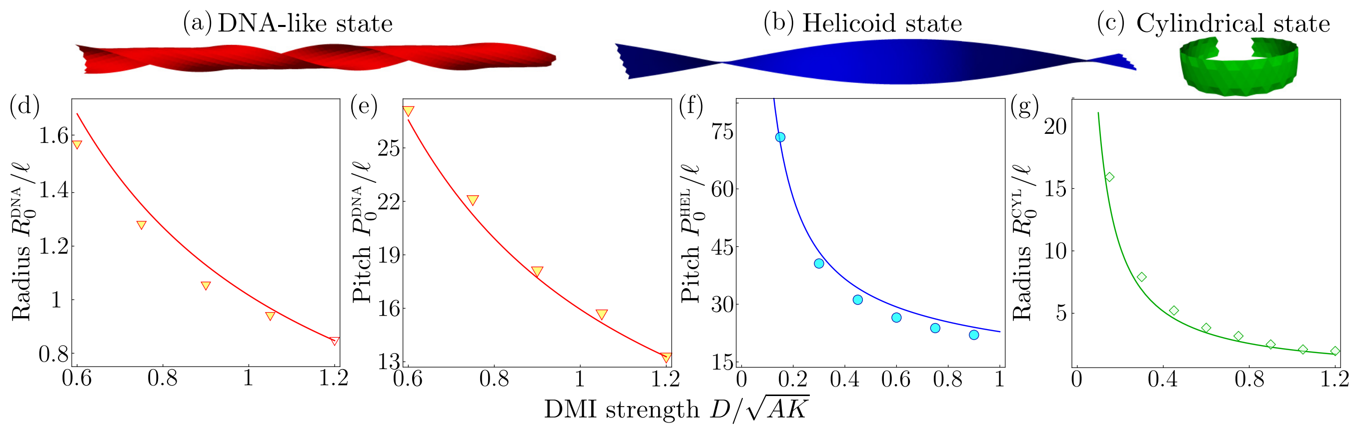


FIG. 2. Shapes and geometrical parameters of flexible ferromagnetic ribbons as functions of DMI strength: (a)–(c) are the ribbon shapes obtained by means of numerical simulations. (d) and (e) are the radius and pitch of the DNA-like state plotted for $A/(Yh^2) = 1$, respectively. (f) Pitch of the helicoid state for $A/(Yh^2) = 0.11$. (g) Radius of the cylindrical state for $A/(Yh^2) = 1$. The red lines in (d) and (e) and the green line in (g) represent analytical predictions (2) and (6), respectively. The blue line in (f) is obtained from solution of the cubic Eq. (S26) in [36]. Symbols correspond to data obtained by means of numerical simulations. The length of ribbons in (d)–(f) is $L = 50\ell$ and $L = 10\ell$ in (g). All data are presented for ribbons with width $w \approx 2\ell$, thickness $h = 0.05\ell$, and Poisson ratio $\nu = 1/3$. The dynamical process of the DMI-induced deformation is illustrated in the Supplemental Material movie [36].

system, one should expect realization of a periodical magnetization distribution due to the 3D deformation of the ribbon. Schematic illustrations of the found DMI-induced deformations of flexible ferromagnetic ribbons are presented in Table I.

Now we utilize the model (1) to provide an analytic description for the DMI-induced flexible ferromagnetic ribbon deformation.

*DMI of Bloch type.* Here we consider DMI in form $\mathcal{E}_{\mathrm{D}} = \mathcal{E}_{\mathrm{D}}^{\mathrm{B}}$. We start with a tangential easy-axial anisotropy ($\boldsymbol{e}_{\mathrm{A}} = \boldsymbol{e}_1$) [49]. Based on our numerical simulations we assume that DMI-induced deformation leads to the formation of two equilibrium states, namely, DNA-like [Fig. 2(a)] and helicoid [Fig. 2(b)] states. We start with a DNA-like state. Such a state is parameterized as $\boldsymbol{\varsigma}^{\mathrm{DNA}}(\xi_1, \xi_2) = R\cos(\rho/R)\hat{\boldsymbol{x}} + R\sin(\rho/R)\hat{\boldsymbol{y}} + (\xi_1\sin\psi + \xi_2\cos\psi)\hat{\boldsymbol{z}}$, where $\rho = \xi_1\cos\psi - \xi_2\sin\psi$, $R$ is a radius of the central line, and $\psi$ is an angle between vector $\boldsymbol{e}_1$ and the $\boldsymbol{xy}$ plane [see Fig. 1(a)]. The pitch of the DNA-like state is $P = 2\pi R\tan\psi$. And the sign of the pitch determines the geometrical chirality $\mathcal{C}^{\mathrm{DNA}} = \mathrm{sgn}P^{\mathrm{DNA}} = \pm 1$. This parametrization results in the Euclidean metrics, therefore this state is free of the stretching (i.e., $g_{\alpha\beta} = \bar{g}_{\alpha\beta}$).

We show [36] that the total energy (1) is minimized by a stationary solution $\boldsymbol{m}_0^{\mathrm{DNA}} = \mathfrak{C}\boldsymbol{e}_1$, where $\mathfrak{C} = \pm 1$ determines whether magnetization is parallel ($\mathfrak{C} = 1$) or antiparallel ($\mathfrak{C} = -1$) to the tangential axis. Equilibrium values for the radius $R$ and pitch $P$ are determined as

$$R_0^{\mathrm{DNA}} = \frac{A}{|D|}\frac{2\sqrt[4]{1+\zeta}}{\sqrt{1+\zeta}-1}, \qquad P_0^{\mathrm{DNA}} = \frac{A}{D}\frac{4\pi\sqrt{1+\zeta}}{\sqrt{1+\zeta}-1}, \tag{2}$$

with $\zeta = 24(1-\nu^2)A/(Yh^2)$. The radius and pitch for the DNA-like state as functions of DMI strength are presented in Figs. 2(d) and 2(e). For the case of relatively large values of Young's modulus $[A/(Yh^2) \ll 1]$ we have $R_0^{\mathrm{DNA}} \propto Yh^2/[6|D|(1-\nu^2)]$ and $P_0^{\mathrm{DNA}} \propto \pi Yh^2/[3D(1-\nu^2)]$.

The energy of the DNA-like state is

$$\frac{E_0^{\mathrm{DNA}}}{hwL} = -\frac{D^2}{4A}\frac{\sqrt{1+\zeta}-1}{\sqrt{1+\zeta}+1} \approx -3(1-\nu^2)\frac{D^2}{Yh^2}. \tag{3}$$

The second equilibrium state is referred to as a helicoid state. Such state can be parametrized in the following way $\boldsymbol{\varsigma}^{\mathrm{HEL}}(\xi_1, \xi_2) = \xi_2[\cos(k\xi_1)\hat{\boldsymbol{x}} + \sin(k\xi_1)\hat{\boldsymbol{y}}] + \xi_1\hat{\boldsymbol{z}}$, where $k$ is a twist parameter of the helicoid ribbon, which results in the pitch $P^{\mathrm{HEL}} = 2\pi/k$. The helical state is also characterized by the geometrical chirality $\mathcal{C}^{\mathrm{HEL}} = \mathrm{sgn}P^{\mathrm{HEL}} = \pm 1$. The metric tensor for this state has a diagonal form $\|g_{\alpha\beta}\| = \mathrm{diag}(1 + k^2\xi_2^2, 1)$. In contrast to the DNA-like state the helicoid geometry has nonzero Gauss curvature. This means that the metric tensor cannot be transformed to the Euclidean form. In our case it results in the stretching term in the energy (1).

By minimizing energy (1), we obtained similar solution for the magnetization as for the DNA-like state [36]: $\boldsymbol{m}_0^{\mathrm{HEL}} = \mathfrak{C}\boldsymbol{e}_1$. The equilibrium value of pitch for the case of narrow ribbons $kw \ll 1$ and large Young's modulus can be determined as

$$P_0^{\mathrm{HEL}} \approx \frac{\pi}{3(1+\nu)}\frac{Yh^2}{D}\left[1 + 12(1+\nu)\frac{A}{Yh^2}\right]. \tag{4}$$

The pitch of the helicoid state as a function of the DMI constant is presented in Fig. 2(f).

The energy of the helicoid state is

$$\frac{E_0^{\mathrm{HEL}}}{hwL} \approx -3(1+\nu)\frac{D^2}{Yh^2}\left[1 - \frac{27}{40}\frac{D^2}{Y^2h^2}\frac{w^4}{h^4}\frac{(1+\nu)^2}{(1-\nu)}\right]. \tag{5}$$

One should note that geometrical chirality of both states (DNA-like and helicoid) does not depend on the magnetization orientation and is defined only by the sign of the DMI constant: $D > 0$ for a left-handed ribbon and $D < 0$ for a right-handed ribbon.

The helicoid state appears due to the realization of a conical phase allowed by the elastic degree of freedom. This state is characterized by nonzero stretching. The competition between the stretching and bending energies results in the appearance of the DNA-like state for the larger $D$. In the limit of small $D$ both energies $E_0^{\mathrm{HEL}} \propto -D^2$ and $E_0^{\mathrm{DNA}} \propto -D^2$ demonstrate quadratic dependence on $D$ and $E_0^{\mathrm{HEL}} < E_0^{\mathrm{DNA}}$. However, for larger $D$ the stretching-induced term $\propto +D^4$ in (5) results in the preferability of the DNA state $E_0^{\mathrm{DNA}} < E_0^{\mathrm{HEL}}$. By comparing the energies of different states, we find the energetically preferable states for different $D$ and $Y$ values. The resulting phase diagrams are presented in Figs. 1(c) and 1(d). There are two phases: (i) The DNA-like state is energetically preferable for relatively large values of $D$ or wide ribbons. (ii) The helicoid state is realized for relatively small values of $D$ or narrow ribbons. The magnetization distribution in both states is uniform in curvilinear reference frame and it is tangential to the ribbon surface. The boundary between two phases can be derived by using the condition $E_0^{\mathrm{HEL}}(D_c, Y) = E_0^{\mathrm{DNA}}(D_c, Y)$ [36]. The spontaneous deformations into the DNA-like and helicoid states are demonstrated in the Supplemental Material movie [36].

*DMI of Néel type.* Here we consider DMI in form $\mathcal{E}_{\mathrm{D}} = \mathcal{E}_{\mathrm{D}}^{\mathrm{N}}$ which is expected to Janus monolayers of $\mathrm{Cr(I,Br)_3}$ and $\mathrm{Cr(I,Cl)_3}$ [43]. For ribbons with tangential easy-axial anisotropy, i.e., easy axis is oriented along the ribbon $\boldsymbol{e}_{\mathrm{A}} = \boldsymbol{e}_1$, the equilibrium magnetization is aligned with the tangential direction and DMI does not deform the shape of the ribbon. While for the easy-normal anisotropy, DMI results in the deformation to the cylindrical structure [see Fig. 2(c)]. This deformation is a limit case of a DNA-like state with $\sin\psi_0^{\mathrm{DNA}} = 0$. The equilibrium value of the radius is [36]

$$R_0^{\mathrm{CYL}} = 2\frac{A}{|D|}\left[1 + \frac{Yh^2}{24A(1+\nu)}\right]. \tag{6}$$

Magnetization in this state is normal to the surface, i.e., $\boldsymbol{m}_0^{\mathrm{CYL}} = \pm\boldsymbol{n}$. The energy of this state behaves as $E_0^{\mathrm{CYL}} \propto -D^2/(Yh^2)$ [36]. The obtained prediction (6) is in good agreement with numerical simulations [see Fig. 2(g)]. One should note, that for ribbons with $L > 2\pi R_0^{\mathrm{CYL}}$ the ribbon formally will wrap itself more than one time. This case should be studied separately. The spontaneous deformation into the cylindrical state is demonstrated in the Supplemental Material movie [36].

For the case of rigid ribbon ($Y \to \infty$) or vanishing DMI ($D \to 0$), one gets values $P_0^{\mathrm{HEL}}$, $P_0^{\mathrm{DNA}}$, $R_0^{\mathrm{DNA}}$, $R_0^{\mathrm{CYL}} \to \infty$, which correspond to the straight ribbon.

*Influence of the external magnetic field.* Finally, we studied the influence of the external magnetic field $\boldsymbol{H}$ on the equilibrium states considered above. The magnetic field was applied along the $\hat{z}$ axis, i.e., $\boldsymbol{H} = H\hat{z}$, for the DNA-like and helicoid states, while for the cylindrical state $\boldsymbol{H} = H\hat{\boldsymbol{x}}$. The interaction with the magnetic field is represented by the Zeeman term with energy density $\mathcal{E}_{\mathrm{Z}} = -M_s\boldsymbol{m}\cdot\boldsymbol{H}$. The influence of the magnetic field was studied by means of the numerical simulations [36].

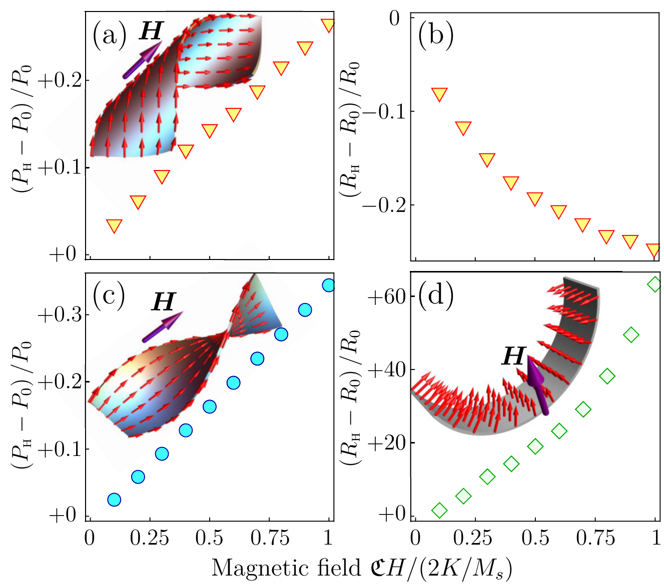


FIG. 3. Influence of the magnetic field on the geometrical parameters of the ribbon: (a),(b) Relative field-induced changes of radius and pitch of the DNA-like state as a function of the applied magnetic field, respectively. (c) Relative field-induced change of the pitch of the helicoid state as a function of the applied field. (d) Relative field-induced change of the radius of the cylindrical state as a function of the applied field. Here $R_{\mathrm{H}}$ and $P_{\mathrm{H}}$ are the radius and pitch of structures in the presence of an external magnetic field, respectively. All data are obtained by means of numerical simulations for ribbons with $w \approx 2\ell$, $h = 0.05\ell$, $A/(Yh^2) = 1$, and $\nu = 1/3$. Insets demonstrate the direction of the magnetic field $\boldsymbol{H}$ with respect to the deformed ribbon and magnetization orientation. Field-induced dynamics is illustrated in the Supplemental Material movie [36].

Typical values of field-induced changes of radii and pitches are presented in Fig. 3. One should note, that the magnitude of the field-induced deformation of the cylindrical state is especially large: the cylinder radius increases by the factor of 60 in our numerical experiments [see Fig. 3(g)]. At the same time, the helicoid and DNA states are more robust, and the relative change of the geometrical parameters does not exceed a few tens of percent.

*Conclusions.* In conclusion, we predict the effect of spontaneous deformation of a flexible ferromagnetic ribbon induced by DMI. The type of deformation depends on the DMI symmetry and equilibrium magnetization distribution (see Table I). For a DMI of Bloch type the deformation is possible only for the tangential magnetization of the ribbon and it is determined by the geometrical, mechanical, and magnetic parameters: a DNA-like state takes place for wide ribbons or relatively large $D$, while a helicoid state is typical for narrow ribbons or relatively small $D$ (see Fig. 1). In both cases the geometrical chirality of the ribbon is determined by the sign of $D$ and does not depend on the magnetization orientation along the ribbon. For the case of the Néel-type DMI there is only one deformed state, namely, the cylindrical state (limit case of the DNA-like state with $\psi = 0$). It takes place only for the ribbons magnetized in normal direction.

Finally, we show that geometrical parameters of the ribbon are significantly influenced by the external magnetic field (see Fig. 3). This feature can be used for control of the nanorobots mechanics.

*Acknowledgments*. We thank U. Nitzsche for technical support and U. Rößler for the helpful discussions. K.V.Y. acknowledges financial support from UKRATOP-project funded by the German Federal Ministry of Education and Research, Grant No. 01DK18002. Yu.G. acknowledges financial support from the Department of Physics and Astronomy of the National Academy of Sciences of Ukraine (Project 6541230). In part, this work was supported by the Alexander von Humboldt Foundation (Research Group Linkage Programme), by the Program of Fundamental Research of the Department of Physics and Astronomy of the National Academy of Sciences of Ukraine (Project No. 0116U003192) and by Taras Shevcheko National University of Kyiv (Project No. 19BF052-01).

[1] D. Makarov, M. Melzer, D. Karnaushenko, and O. G. Schmidt, Shapeable magnetoelectronics, Appl. Phys. Rev. **3**, 011101 (2016).

[2] P. Sheng, B. Wang, and R. Li, Flexible magnetic thin films and devices, J. Semicond. **39**, 011006 (2018).

[3] J. Wang, M.-F. Lin, S. Park, and P. S. Lee, Deformable conductors for human–machine interface, Mater. Today **21**, 508 (2018).

[4] W. Hu, G. Z. Lum, M. Mastrangeli, and M. Sitti, Small-scale soft-bodied robot with multimodal locomotion, Nature (London) **554**, 81 (2018).

[5] G. Z. Lum, Z. Ye, X. Dong, H. Marvi, O. Erin, W. Hu, and M. Sitti, Shape-programmable magnetic soft matter, Proc. Natl. Acad. Sci. USA **113**, E6007 (2016).

[6] Y. Kim, H. Yuk, R. Zhao, S. A. Chester, and X. Zhao, Printing ferromagnetic domains for untethered fast-transforming soft materials, Nature (London) **558**, 274 (2018).

[7] H. Lu, M. Zhang, Y. Yang, Q. Huang, T. Fukuda, Z. Wang, and Y. Shen, A bioinspired multilegged soft millirobot that functions in both dry and wet conditions, Nat. Commun. **9**, 3944 (2018).

[8] J. Zhang and E. Diller, Untethered miniature soft robots: Modeling and design of a millimeter-scale swimming magnetic sheet, Soft Robotics **5**, 761 (2018).

[9] J. Kim, S. E. Chung, S.-E. Choi, H. Lee, J. Kim, and S. Kwon, Programming magnetic anisotropy in polymeric microactuators, Nat. Mater. **10**, 747 (2011).

[10] M. Medina-Sánchez, V. Magdanz, M. Guix, V. M. Fomin, and O. G. Schmidt, Swimming microrobots: Soft, reconfigurable, and smart, Adv. Funct. Mater. **28**, 1707228 (2018).

[11] H. Ceylan, I. C. Yasa, O. Yasa, A. F. Tabak, J. Giltinan, and M. Sitti, 3D-printed biodegradable microswimmer for theranostic cargo delivery and release, ACS Nano **13**, 3353 (2019).

[12] H. Singh, P. E. Laibinis, and T. A. Hatton, Synthesis of flexible magnetic nanowires of permanently linked core-shell magnetic beads tethered to a glass surface patterned by microcontact printing, Nano Lett. **5**, 2149 (2005).

[13] J. Thévenot, H. Oliveira, O. Sandre, and S. Lecommandoux, Magnetic responsive polymer composite materials, Chem. Soc. Rev. **42**, 7099 (2013).

[14] G. Herzer, Modern soft magnets: Amorphous and nanocrystalline materials, Acta Mater. **61**, 718 (2013).

[15] R. Geryak and V. V. Tsukruk, Reconfigurable and actuating structures from soft materials, Soft Matter **10**, 1246 (2014).

[16] J. Townsend, R. Burtovyy, Y. Galabura, and I. Luzinov, Flexible chains of ferromagnetic nanoparticles, ACS Nano **8**, 6970 (2014).

[17] E. Lopatina, I. Soldatov, V. Budinsky, M. Marsilius, L. Schultz, G. Herzer, and R. Schäfer, Surface crystallization and magnetic properties of $Fe_{84.3}Cu_{0.7}Si_4B_8P_3$ soft magnetic ribbons, Acta Mater. **96**, 10 (2015).

[18] D. Romeis, P. Metsch, M. Kästner, and M. Saphiannikova, Theoretical models for magneto-sensitive elastomers: A comparison between continuum and dipole approaches, Phys. Rev. E **95**, 042501 (2017).

[19] P. Vázquez-Montejo and M. O. de la Cruz, Flexible paramagnetic membranes in fast precessing fields, Phys. Rev. E **98**, 032603 (2018).

[20] C. A. Brisbois, M. Tasinkevych, P. Vázquez-Montejo, and M. O. de la Cruz, Actuation of magnetoelastic membranes in precessing magnetic fields, Proc. Natl. Acad. Sci. USA **116**, 2500 (2019).

[21] R. Zhao, Y. Kim, S. A. Chester, P. Sharma, and X. Zhao, Mechanics of hard-magnetic soft materials, J. Mech. Phys. Solids **124**, 244 (2019).

[22] A. A. Ovchinnikov and V. N. Spector, Organic ferromagnets. new results, Synth. Met. **27**, 615 (1988).

[23] J. S. Miller, A. J. Epstein, and W. M. Reiff, Molecular/organic ferromagnets, Science **240**, 40 (1988).

[24] F. Palacio, J. Ramos, and C. Castro, Magnetic polymers, Mol. Cryst. Liq. Cryst. Sci. Technol., Sect. A **232**, 173 (1993).

[25] J. S. Miller, Organic magnets—A history, Adv. Mater. **14**, 1105 (2002).

[26] R. Podgajny, M. Bałanda, M. Sikora, M. Borowiec, L. Spałek, C. Kapusta, and B. Sieklucka, Cobalt(II) octacyanotungstate(V) organic–inorganic hybrid ferromagnetic materials with pyrazine and 4, 4′-bipyridine, Dalton Trans. **23**, 2801 (2006).

[27] L. D. Barron, Chirality and magnetism shake hands, Nat. Mater. **7**, 691 (2008).

[28] J. S. Miller, Magnetically ordered molecule-based materials, Chem. Soc. Rev. **40**, 3266 (2011).

[29] J. S. Miller, Organic- and molecule-based magnets, Mater. Today **17**, 224 (2014).

[30] J. Mahmood, J. Park, D. Shin, H.-J. Choi, J.-M. Seo, J.-W. Yoo, and J.-B. Baek, Organic ferromagnetism: Trapping spins in the glassy state of an organic network structure, Chem **4**, 2357 (2018).

[31] P. Bujak, I. Kulszewicz-Bajer, M. Zagorska, V. Maurel, I. Wielgus, and A. Pron, Polymers for electronics and spintronics, Chem. Soc. Rev. **42**, 8895 (2013).

[32] R. Dandoloff, S. Villain-Guillot, A. Saxena, and A. R. Bishop, Violation of Self-Duality for Topological Solitons Due to Soliton-Soliton Interaction on a Cylindrical Geometry, Phys. Rev. Lett. **74**, 813 (1995).

[33] A. Saxena and R. Dandoloff, Curvature-induced geometrical frustration in magnetic systems, Phys. Rev. B **55**, 11049 (1997).

[34] A. Saxena, R. Dandoloff, and T. Lookman, Deformable curved magnetic surfaces, Physica A (Amsterdam, Neth.) **261**, 13 (1998).

[35] Y. Gaididei, K. V. Yershov, D. D. Sheka, V. P. Kravchuk, and A. Saxena, Magnetization-induced shape transformations in flexible ferromagnetic rings, Phys. Rev. B **99**, 014404 (2019).

[36] See Supplemental Material at http://link.aps.org/supplemental/10.1103/PhysRevB.100.140407 for details of analytical calculations and movies, which includes Refs. [37,50–54].

[37] E. Efrati, E. Sharon, and R. Kupferman, Elastic theory of unconstrained non-Euclidean plates, J. Mech. Phys. Solids **57**, 762 (2009).

[38] S. Armon, E. Efrati, R. Kupferman, and E. Sharon, Geometry and mechanics in the opening of chiral seed pods, Science **333**, 1726 (2011).

[39] D. Cortes-Ortuno and P. Landeros, Influence of the Dzyaloshinskii-Moriya interaction on the spin-wave spectra of thin films, J. Phys.: Condens. Matter **25**, 156001 (2013).

[40] A. N. Bogdanov and U. K. Rößler, Chiral Symmetry Breaking in Magnetic Thin Films and Multilayers, Phys. Rev. Lett. **87**, 037203 (2001).

[41] A. Thiaville, S. Rohart, É. Jué, V. Cros, and A. Fert, Dynamics of Dzyaloshinskii domain walls in ultrathin magnetic films, Europhys. Lett. **100**, 57002 (2012).

[42] H. Yang, A. Thiaville, S. Rohart, A. Fert, and M. Chshiev, Anatomy of Dzyaloshinskii-Moriya Interaction at Co/Pt Interfaces, Phys. Rev. Lett. **115**, 267210 (2015).

[43] C. Xu, J. Feng, H. Xiang, and L. Bellaiche, Magnetic skyrmion state in Janus monolayers of chromium trihalides $Cr(I, X)_3$, arXiv:1906.04336.

[44] D.-H. Kim, M. Haruta, H.-W. Ko, G. Go, H.-J. Park, T. Nishimura, D.-Y. Kim, T. Okuno, Y. Hirata, Y. Futakawa, H. Yoshikawa, W. Ham, S. Kim, H. Kurata, A. Tsukamoto, Y. Shiota, T. Moriyama, S.-B. Choe, K.-J. Lee, and T. Ono, Bulk Dzyaloshinskii–Moriya interaction in amorphous ferrimagnetic alloys, Nat. Mater. **18**, 685 (2019).

[45] I. E. Dzyaloshinskii, Theory of helicoidal structures in antiferromagnets. I. Nonmetals, ZhETF **46**, 1420 (1964) [Sov. Phys. JETP **19**, 960 (1964)].

[46] I. E. Dzyaloshinskii, The theory of helicoidal structures in antiferromagnets. II. Metals, ZhETF **47**, 336 (1965) [Sov. Phys. JETP **20**, 223 (1965)].

[47] A. N. Bogdanov, U. K. Rössler, and C. Pfleiderer, Modulated and localized structures in cubic helimagnets, Physics B (Amsterdam, Neth.) **359-361**, 1162 (2005).

[48] M. Heide, G. Bihlmayer, and S. Blügel, Non-planar Dzyaloshinskii spirals and magnetic domain walls in non-centrosymmetric systems with orthorhombic anisotropy, J. Nanosci. Nanotechnol. **11**, 3005 (2011).

[49] For ribbons with DMI of Bloch type and normal easy-axial anisotropy, i.e., $\boldsymbol{e}_{\mathrm{A}} = \boldsymbol{n}$, the equilibrium magnetization is aligned with the normal direction and DMI does not deform the shape of the ribbon.

[50] B. A. Dubrovin, A. T. Fomenko, and S. P. Novikov, *Modern Geometry-Methods and Applications: Part I. The Geometry of Surfaces, Transformation Groups, and Fields*, 2nd ed., Graduate Texts in Mathematics 93 Vol. 1 (Springer, New York, 1984).

[51] Y. Gaididei, V. P. Kravchuk, and D. D. Sheka, Curvature Effects in Thin Magnetic Shells, Phys. Rev. Lett. **112**, 257203 (2014).

[52] D. D. Sheka, V. P. Kravchuk, and Y. Gaididei, Curvature effects in statics and dynamics of low dimensional magnets, J. Phys. A: Math. Theor. **48**, 125202 (2015).

[53] V. P. Kravchuk, U. K. Rößler, O. M. Volkov, D. D. Sheka, J. van den Brink, D. Makarov, H. Fuchs, H. Fangohr, and Y. Gaididei, Topologically stable magnetization states on a spherical shell: Curvature-stabilized skyrmions, Phys. Rev. B **94**, 144402 (2016).

[54] V. P. Kravchuk, D. D. Sheka, A. Kákay, O. M. Volkov, U. K. Rößler, J. van den Brink, D. Makarov, and Y. Gaididei, Multiplet of Skyrmion States on a Curvilinear Defect: Reconfigurable Skyrmion Lattices, Phys. Rev. Lett. **120**, 067201 (2018).